

Equilibrium spin-glass transition of magnetic dipoles with random anisotropy axes

Julio F. Fernández¹

¹*Instituto de Ciencia de Materiales de Aragón, CSIC and Universidad de Zaragoza, 50009-Zaragoza, Spain**

(Dated: November 1, 2018)

We study fully occupied lattice systems of classical magnetic dipoles which point along random axes. Only dipolar interactions are considered. From tempered Monte Carlo simulations, we obtain numerical evidence that supports the following conclusions: in three dimensions, (a) there is an equilibrium spin glass phase at temperatures below T_c , where $k_B T_c = (0.86 \pm 0.07)\varepsilon_d$ and ε_d is a nearest neighbor dipole-dipole interaction energy, (b) in the spin glass phase the overlap parameter is approximately given by $\sqrt{1 - T/T_c}$, and (c) the correlation length ξ diverges at T_c with a critical exponent $\nu = 1.5 \pm 0.5$; in two dimensions ξ diverges at or near $T = 0$ and $\nu = 3 \pm 1$.

PACS numbers: 75.45.+j, 75.50.Xx, 75.70.-i

Keywords:

I. INTRODUCTION

Several decades after the experimental discovery of spin glasses,¹ convincing numerical evidence for an equilibrium phase transition between the paramagnetic and spin-glass phases of the random bond Ising^{2,3} model in three dimensions is at last available. Somewhat more controversial evidence is also available for the Heisenberg model.^{4,5} No such results that we know of exist for systems in which dipole-dipole interactions dominate. This is in spite of all the interest that has arisen in these systems since nanosized magnetic particles have become experimentally available.⁶ Randomness, one of the two essential ingredients for spin-glass behavior, can arise from spatial disorder,⁷ which in turn, most often, brings about random magnetic anisotropies. One might naively expect that the long range nature of dipolar interactions would only strengthen the spin glass phase that is observed in the random (nearest neighbor) bond Ising model. However, recent results from computer simulations suggest that an equilibrium spin glass phase does not obtain in a spatially disordered system of magnetic dipoles which point along parallel axes.⁸ The reason for this somewhat unexpected result may be the nature of frustration that is peculiar to dipolar systems. In them, there is frustration whether they are spatially ordered or not. It is precisely because of this that ferro- or antiferro-magnetism prevails in well ordered crystalline dipolar systems depending delicately on lattice geometry.⁹ On the other hand, spin-glass like behavior has been observed in experiments^{10,11,12} and in simulations^{13,14,15,16,17} of dipolar systems with random anisotropies, but all this evidence comes from *out of equilibrium* phenomena, as exhibited by time dependent susceptibilities, nonexponential relaxation, and aging.¹⁷

We study the equilibrium behavior of systems of interacting magnetic dipoles which are oriented along random anisotropy axes in two and three dimensions (D). This random axes dipolar (RAD) model is like the old model of Harris, Plischke, and Zuckerman,¹⁸ except that we deal with dipole-dipole, rather than nearest neighbor

(nn) interactions. Some motivation for the RAD model comes from the fact that anisotropy energies in nanoparticle assemblies are often¹⁹ much larger than the dipole-dipole interaction energy between two nearest neighbors. As in an Ising model, spins in the RAD model can only point “up” or “down” along each one of their own axes, as is discussed in Refs. [16,20,21]. Two independent random numbers per site are needed to determine all axes directions, which is the same number as for a nn random bond Ising model on a square lattice, though the interaction range is of course quite different.

When we simulate the time evolution of the RAD model, we flip each spin up and down along its own axis. We thus make no attempt to simulate how each individual spin overcomes large anisotropy barriers. Rather, we expect our simulations to mimic the collective time evolution effects that follow after single spin energy barriers are surmounted, as illustrated in Figs. 1 and 2 of Ref. [14]. Anyway, our main interest does not lie in the time dependent properties of the RAD model, but in its equilibrium behavior, which must clearly be the same as for a system of magnetic dipoles under a dominant anisotropy with random axes.

A summary of our results follows. We first illustrate advantages of tempered²² Monte Carlo (TMC) over Metropolis²³ Monte Carlo (MMC) simulations for the calculation of equilibrium behavior. This includes a comparison of the time dependent magnetic susceptibility χ (from MMC runs), which is characteristic of spin glasses, for the RAD model in 2D, with equilibrium results that follow from TMC simulations. We obtain equilibrium results (from TMC simulations) for systems of L^d spins (d is the lattice dimension) for $d = 2$ and $d = 3$, for $L = 4, 8, 16$ and for $L = 4, 6, 8, 12$, respectively. Simulations of larger systems are very time consuming, because running times grow as L^{2d} for systems with *dipolar* interactions. Extrapolations to the $L \rightarrow \infty$ limit point to the following conclusions. In three dimensions (3D), the paramagnetic phase covers the $T > T_c$ range, where T is the temperature, $T_c = (0.86 \pm 0.07)\varepsilon_d/k_B$, k_B is Boltzmann’s constant, and ε_d is a dipole-dipole nn interaction energy which is defined below, in Sec. II A. For

$T < T_c$, there is an equilibrium spin glass phase. In it, the overlap parameter, as defined in Sec. II C, is approximately given by $\sqrt{1 - T/T_c}$. From our results we cannot quite conclude whether the droplet^{24,25} or RSB^{25,26} picture describes the RAD spin glass in 3D. Results for the correlation length ξ , are consistent with $\xi \sim (T - T_c)^{-\nu}$, where $T_c \simeq 0.88$ and $\nu = 1.5 \pm 0.5$.²⁷ In 2D, the paramagnetic phase covers the $T \gtrsim 0$ range, though we cannot rule out a spin glass phase below $T \simeq 0.1$. Results for the correlation length ξ are consistent with $\xi \sim T^{-\nu}$, where $\nu = 3 \pm 1$.

II. MODEL AND METHOD

A. Model

To define the model, let

$$\mathcal{H} = \frac{1}{2} \sum_{ij} \sum_{\alpha\beta} T_{ij}^{\alpha\beta} S_i^\alpha S_j^\beta \quad (1)$$

be its Hamiltonian, where S_i^α is the α (one of three) component of the classical spin on a cubic lattice site i ,

$$T_{ij}^{\alpha\beta} = \varepsilon_d (a/r_{ij})^3 (\delta_{\alpha\beta} - 3r_{ij}^\alpha r_{ij}^\beta / r_{ij}^2), \quad (2)$$

r_{ij} is the distance between i and j , ε_d is an energy, and a a nn distance. Each spin points along a randomly chosen direction. More precisely, let \mathbf{u}_j be a 3-component vector chosen randomly for each i from a spherically uniform distribution of unit vectors, and let $\sigma_j = \pm 1$ at each site, such that $\mathbf{S}_j = \mathbf{u}_j \sigma_j$. Then, \mathcal{H} becomes,

$$\mathcal{H} = -\frac{1}{2} \sum_{ij} J_{ij} \sigma_i \sigma_j, \quad (3)$$

where $J_{ij} = -\sum_{\alpha,\beta} T_{ij}^{\alpha\beta} u_i^\alpha u_j^\beta$. Thus, the RAD model is an Ising model whose bonds J_{ij} are determined by the dipole-dipole terms $T_{ij}^{\alpha\beta}$ and the set of 3-component randomly oriented unit vectors $\{\mathbf{u}_j\}$.

We use periodic boundary conditions in 2D and 3D. Simple cubic lattices and zero applied magnetic field H are assumed throughout. We only work with L^d box-like systems, and let dipole-dipole interactions act between each spin and all other spins within an L^d box centered on it. Because of the long range nature of dipolar interactions, contributions from beyond this box would have to be taken into account (by some scheme, such as Ewald's summation) if spins were to point in any one preferred direction. They do not do so in this (nonferromagnetic) model as long as $H = 0$. The boundary conditions as well as the L^d box scheme we use here are as in Refs. [9,28,29]. Finally, it is worth recalling that thermal equilibrium results obtained for $H=0$ for large cubic-shaped systems can, by virtue of Griffiths theorem³⁰ be generalized to other shapes in three dimensions.

From here on, all temperatures are given in terms of ε_d/k_B , where k_B is Boltzmann's constant.

B. Monte Carlo

Let us first specify how we update the state of the system in all Monte Carlo evolutions. Initially, we compute the dipolar field at each site. Throughout a computer run, tables of all spins and dipolar fields are kept. Dipolar fields are updated throughout all sites in the system whenever a spin is flipped. Thus, no computer time is wasted whenever an attempt to flip a spin ends in failure. This becomes important at low temperatures.

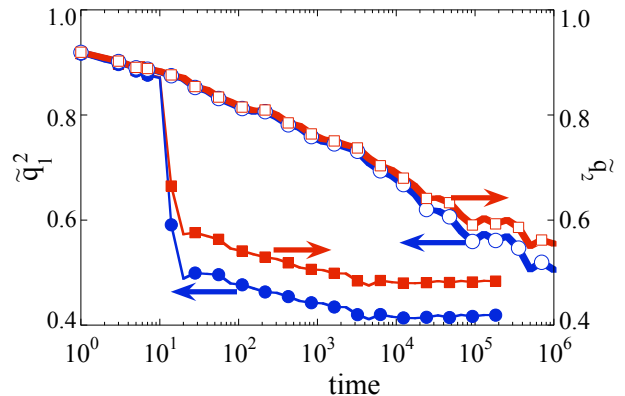


FIG. 1: (Color online) \tilde{q}_1^2 and \tilde{q}_2^2 vs time for systems of $6 \times 6 \times 6$ spins at $T = 0.5$. \square and \circ are for \tilde{q}_2^2 and \tilde{q}_1^2 , respectively. They both follow from the MMC algorithm. On the other hand, \blacksquare and \bullet are also for \tilde{q}_2^2 and \tilde{q}_1^2 , respectively, but they both follow from the TMC algorithm. All data points stand for averages over 200 samples, each with different random anisotropy axes. All systems were allowed to evolve for over 10^5 MCS before any measurements were taken.

The idea behind the tempered Monte Carlo algorithm,²² is as follows. Consider two systems, 2 and 1, in thermal equilibrium, not among themselves but each one of them with its own heat bath, at temperatures T_1 and T_2 , respectively. Let $T_2 > T_1$, and let E_2 and E_1 be the energies of systems 1 and 2 at some given time. In the TMC algorithm, the states of two systems are exchanged with a certain probability p at some specified times. It follows straightforwardly that the canonical thermal probability distributions for systems 1 and 2 are unchanged if $p = 1$ if $E_2 \leq E_1$, and $p = \exp[(\beta_1 - \beta_2)(E_1 - E_2)]$ if $E_2 > E_1$, where $\beta_k = 1/T_k$ for $k = 1, 2$.²²

We do TMC simulations on k identical systems at temperatures $T + n\Delta T$, where $n = 1, 2, \dots, k$, with initially independent random spin configurations, and let all systems evolve in time following the MMC algorithm for a number \tilde{n} of consecutive MMC sweeps. (We choose $\tilde{n} = 10$ throughout.) After every \tilde{n} MMC sweeps, pairs of systems are given a chance to exchange energy, following the above given rule. More specifically, systems $2n$ and $2n + 1$, for $n = 0, 1, 2, \dots$, are allowed to exchange states at $j\tilde{n}$ times, where $j = 1, 2, \dots$, and systems $2n$ and $2n - 1$, for $n = 1, 2, \dots$, are allowed to exchange states at $(j + 1/2)\tilde{n}$ times. We choose ΔT as follows. Fre-

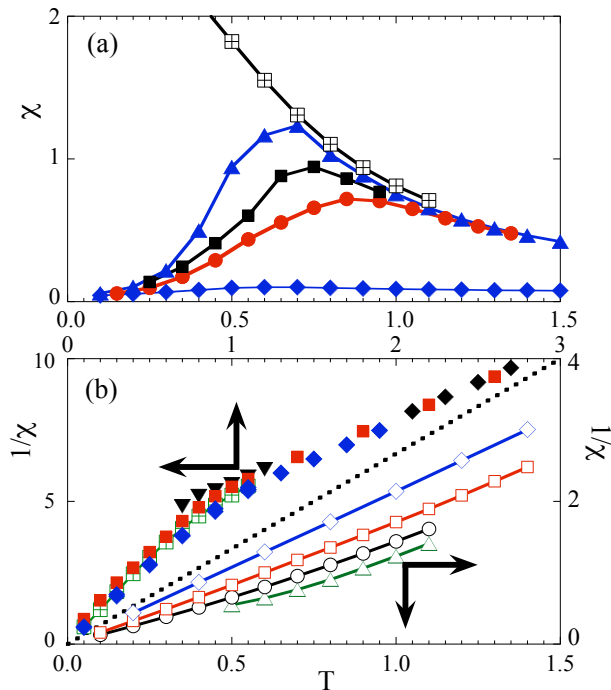


FIG. 2: (Color online) (a) In plane ($\chi_{||}$) and out of plane (χ_{\perp}) susceptibilities vs T for 2D systems of $L \times L$ spins. \blacktriangle , \blacksquare , and \bullet are for $\chi_{||}$, from MMC runs of 10^4 , 10^5 , and 10^6 MCS, respectively. The low lying string of \blacklozenge symbols is for χ_{\perp} . \boxplus is for data points which follow from TMC for $\chi_{||}$. Finally, all \boxplus , \blacktriangle , and \blacklozenge are for $L = 32$ and the rest of data points are for $L = 16$. Error bars are roughly given by icon sizes. (b) $1/\chi$ vs T , from TMC simulations. All data points above (below) the diagonal dotted line are for 3D (2D) systems. \diamond , \square , \circ , and \triangle are for $L = 4, 8, 16$, and 32 , respectively. \blacklozenge , \boxplus , \blacksquare , and \blacktriangledown are for $L = 4, 6, 8$, and 12 , respectively. Parameters for TMC runs are given in table I.

quent exchanges take place if the energy difference ΔE between systems $2n$ and $2n \pm 1$ is not much larger than the energy fluctuations.²² On the other hand, we know from our own simulations of the RAD model, that the specific heat C fulfills $C \approx T^2$ for $T \lesssim 0.6$ and $C \lesssim T^2$ for all $0 < T$, both in 2D and 3D. Using $C \lesssim T^2$, one obtains $\Delta T \lesssim 1/\sqrt{N}$, which is the desired condition.

How much faster stationary states are approached in TMC than in MMC simulations is illustrated in Fig. 1, where plots of \tilde{q}_1^2 and \tilde{q}_2 (defined in Sec. II C) vs time are shown, using data points from both MMC and TMC. For further comparison, results obtained for the susceptibility χ from MMC and TMC simulations are shown in Fig. 2a. All data points, except the low lying branch, are for the “in plane” susceptibility $\chi_{||}$, that is, the linear in plane magnetization response to an in plane applied magnetic field. The low lying branch in Fig. 2a is for the “out of plane” linear susceptibility χ_{\perp} . (As is well known, dipolar interactions lead to “shape anisotropy”, which for 2D gives $\chi_{||} \gg \chi_{\perp}$.²⁸) We often write χ for $\chi_{||}$. All data points in Figs. 2a, 2b, and 2c follow from measurements of magnetization fluctuations in $H = 0$.

The data points from MMC simulations clearly exhibit time dependent effects that are sometimes associated with spin glasses. The peak in $\chi_{||}$ shifts to lower values of T as the number of MCS increases. This is as expected from a spin glass. Results from MMC in 3D (not shown) do not differ qualitatively from the results shown in Fig. 2a for 2D. Finally, equilibrium susceptibilities that follow from magnetization fluctuations in TMC runs are shown in Fig. 2b for system of various sizes, in 2D and in 3D.

C. Overlaps

We next define the equilibrium quantities we calculate. Following the original idea of Edwards and Anderson,³¹ consider two identical replicas, 1 and 2, of a system. Both replicas have the same set of anisotropy axes but evolve in time independently, starting from arbitrarily different initial states.³¹ Let

$$\phi_j = \sigma_j^{(1)} \sigma_j^{(2)}, \quad (4)$$

where $\sigma_j^{(1)}$ and $\sigma_j^{(2)}$ be the spins on site j of replicas 1 and 2, and

$$q = L^{-d} \sum_j \phi_j. \quad (5)$$

We also define the moments of q , $q_k = \langle |q|^k \rangle$, for $k = 1, 2$ and 4 , where $\langle \dots \rangle$ stands for an average over equilibrium states of a large number N_s of replica pairs with independent random axes orientations. Note we use an absolute value in the definition of q_1 . We refer to q_1 as the overlap parameter. The spin glass susceptibility is given by $L^d q_2$.

Recall that if the probability distribution $P(q)$ in the spin glass phase differs from zero only in a vanishingly small neighborhood of some $q = \pm q_0$, where $0 < q_0 \leq 1$, as in the droplet model,^{24,25} then, $q_2 = q_1^2 > 0$. On the other hand, if $P(q) \neq 0$ over a finite range of q values, as in the RSB scheme,^{25,26} then $q_2 > q_1^2$.

In order to keep track of time evolutions, we also define $\tilde{\phi}_j(t_0, t) = \sigma_j(t_0) \sigma_j(t_0 + t)$, in close analogy with the definition of Eq. 4, except that both $\sigma_j(t_0)$ and $\sigma_j(t_0 + t)$ are the same spin, at site j , at times t_0 and $t_0 + t$, respectively. We also define $\tilde{q}(t, t_0) = L^{-d} \sum_j \tilde{\phi}_j(t, t_0)$, and the moments \tilde{q}_k in obvious analogy to q_k . No measurement is ever taken, neither for the calculation of q_k nor for $\tilde{q}_k(t_0, t_0 + t)$, in any simulation up to time t_0 . The question is how to choose t_0 . Obviously, the $t \rightarrow \infty$ limit of $\tilde{q}_k(t, t_0)$ depends on t_0 . Indeed, aging is the outcome of a rather long lasting dependence on t_0 .^{12,13,17} For equilibrium results, we choose sufficiently large values of t_0 in order that $\tilde{q}_k(t, t_0)$ reach steady state before $t = t_0$. Failure to do so would imply that equilibrium had not been reached by t_0 , after which time measurements had been taken. We thus (a) let t_0 be halfway to

TABLE I: TMC simulation parameters.

d, L	2, 4	2, 8	2, 16	2, 32	3, 4	3, 6	3, 8	3, 12
N_s	1000	600	300	100	1800	800	400	175
ΔT	0.1	0.1	0.1	0.05	0.1	0.1	0.05	0.05
MCS	10^4	10^5	10^5	10^5	4×10^4	2×10^5	2×10^5	2×10^5

the end of each MC run, that is, we let $t_0 = t_f$, where $2t_f$ is the total number of MC sweeps taken in any given run, starting from a random spin configuration, and (b) let t_f be sufficiently large for \tilde{q}_k to have reached steady state by the end of the run. For short, we write \tilde{q}_k for $\tilde{q}_k(t_f/2, t_f)$. All of this is necessary but not sufficient. Conceivably, an exceedingly fast initial evolution away from a disordered state at an early t_0 could drive $\tilde{q}_k(t_0)$ to a null value, long before equilibrium was reached. On the other hand, the value of q_k , averaged over the time interval (t_0, t_f) , would still depend on t_f . Therefore, for equilibrium calculations we choose t_0 (and therefore t_f) sufficiently long for \tilde{q}_k to become equal to q_k . For comparison, equilibrium data points for both q_k and \tilde{q}_k are sometimes displayed jointly.

III. EQUILIBRIUM RESULTS

We report our equilibrium results in this section. The relevant parameters for all TMC simulations from which these results follow can be found in Table I.

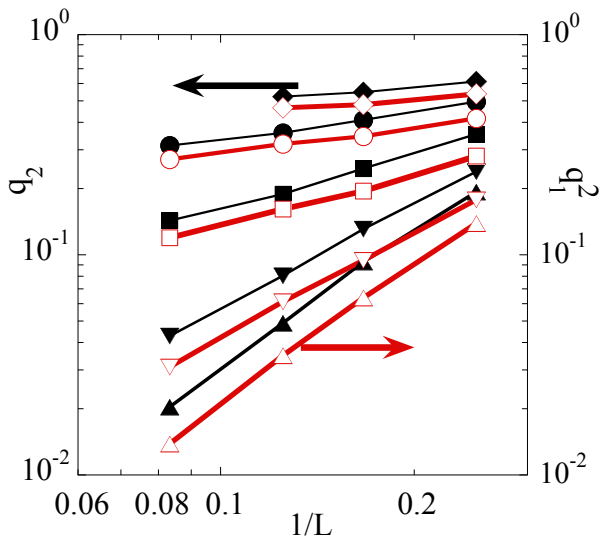


FIG. 3: (Color online) Log-log plots of q_2 (black) and q_1^2 (red) vs $1/L$ in 3D. Closed and open icons are for q_2 and q_1^2 , respectively. \blacklozenge and \diamond are for $T = 0.45$, \bullet and \circ are for $T = 0.6$, \blacksquare and \square are for $T = 0.8$, \blacktriangledown and \triangledown are for $T = 1.0$, and \blacktriangle and \triangle are for $T = 1.1$. Lines are guides to the eye.

Plots of equilibrium values of q_2 and q_1^2 vs $1/L$ are shown in Fig. 3 for systems in 3D at various temper-

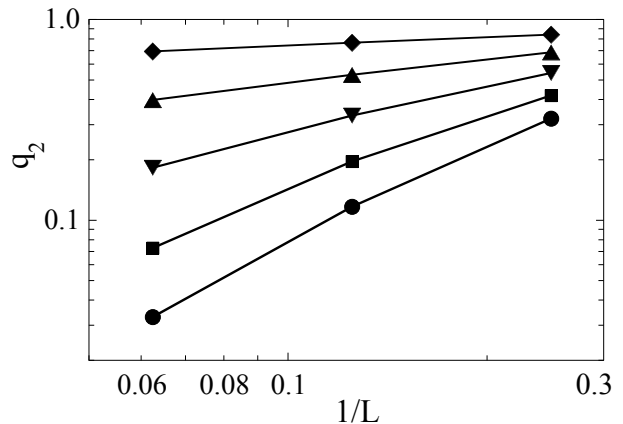


FIG. 4: Plots of q_2 vs $1/L$ in 2D for $T=0.2$ (\blacklozenge), 0.4 (\blacktriangle), 0.6 (\blacktriangledown), 0.8 (\blacksquare), 1.0 (\bullet). Lines are guides to the eye.

atures. For $T \lesssim 1$ ($T \gtrsim 1$), q_2 and q_1^2 curve upward (downward). This suggests $T_c \sim 1$. Extrapolations performed on linear plots (not shown) of q_2 and q_1^2 vs $1/L$ give $1/L \rightarrow 0$ values that are well fitted by

$$q_1^2 = 1 - \frac{T}{T_c}, \quad (6)$$

for $T < T_c$, and a value of T_c that is well within errors of (the value we find below) $T_c = 0.86 \pm 0.07$. In addition, q_2 and q_1^2 extrapolate to roughly the same value, for $T < T_c$. This would be in accordance with the droplet model of spin glasses. However, for reasons given below, this is not a firm conclusion.

In principle, the critical exponent η can be obtained from the plots of q_2 vs $1/L$ shown in Fig. 3, making use of $q_2 \sim 1/L^{d-2+\eta}$ at T_c , which follows from finite size scaling.^{2,34,35} In fact, however, no meaningful number was obtained for η , because the errors turned out to be too large.

Similar plots of q_2 and q_1^2 vs $1/L$ for 2D are shown in Fig. 4. They clearly suggest that, at least for $T \gtrsim 0.4$, $q_2 \rightarrow 0$ as $1/L \rightarrow 0$.

In order to examine the data we have for q_1 and q_2 in a slightly different way, we define,

$$u_{12} = \frac{2}{\pi - 2} \left(\frac{\pi}{2} - \frac{q_2}{q_1^2} \right). \quad (7)$$

Note that u_{12} is scale free, and is consequently only a function of ξ/L , according to finite size scaling (FSS) theory.^{2,34,35} u_{12} is analogous to Binder's ratio u_{24} , which is defined in terms of q_4 and q_2 .³⁶ Clearly, $u_{12} = 1$ for the droplet model. On the other hand $u_{12} = 0$ for a macroscopic paramagnetic system, since q is normally distributed then, as follows from the central limit theorem and the fact that ξ is finite in a paramagnet.

Replacement of q_k by \tilde{q}_k for all k in Eq. (7) gives the definition of \tilde{u}_{12} .

From TMC simulations we obtain the equilibrium results for the RAD model in 3D that are shown in Fig.

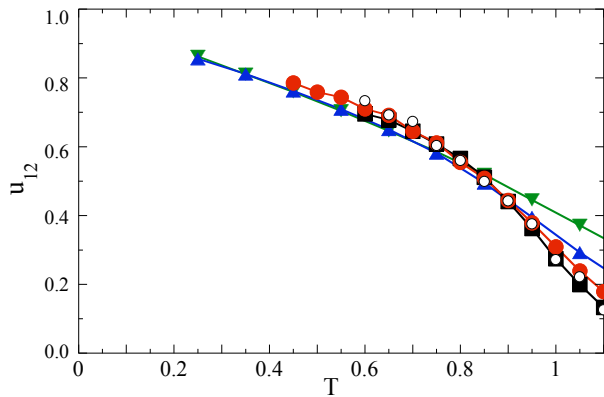


FIG. 5: (Color online) u_{12} vs T for systems of $L \times L \times L$ spins in 3D. ∇ , \blacktriangle , \bullet , and \blacksquare are for $L = 4, 6, 8$, and 12 , respectively. In addition, data points (\circ) for \tilde{u}_{12} are given for $L = 12$. Lines are guides to the eye. Error bars are roughly given by the icon sizes.

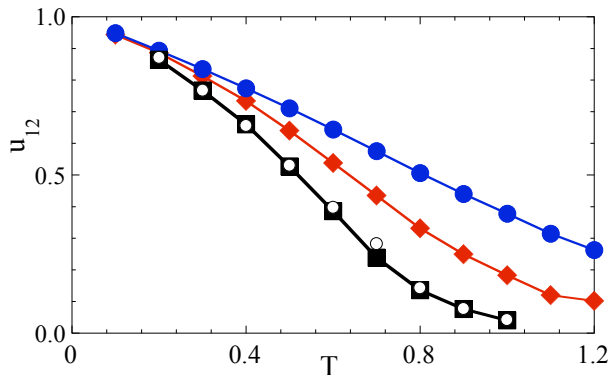


FIG. 6: (Color online) Plot of u_{12} vs T for 2D systems of $L \times L$ spins, for $L = 4$ (\bullet), $L = 8$ (\blacklozenge), and $L = 16$ (\blacksquare). Open icons (\circ) stand for \tilde{u}_{12} for $L = 16$. Lines are guides to the eye. Parameters for all (TMC) runs are given in table I. Icons are approximately of error bar size.

5. Data points for \tilde{u}_{12} are also shown for $L = 12$ in Fig. 5 in order to illustrate the kind of agreement we obtain between u_{12} and \tilde{u}_{12} . It is not clear in Fig. 5 whether u_{12} becomes approximately independent of L or keeps increasing with L for larger values of L and $T \lesssim 0.9$. Size independence then implies $q_2/q_1^2 \simeq 1 + 0.3T$ for $T < T_c$. On the other hand, $u_{12} \rightarrow 1$ as $L \rightarrow \infty$, would give $q_2 \simeq q_1^2$ for macroscopic sizes, which would be in agreement with the tentative inference we drew from Fig. 3. We are thus led to

$$1 \leq \frac{q_2}{q_1^2} \lesssim 1 + 0.3T \quad (8)$$

for macroscopic sizes, which does not discriminate between the Droplet and RSB pictures of the RAD model.

For $T > 0.9$ we have plotted (not shown) u_{12} vs $1/L$, using data points from Fig. 5. Such plots point to $u_{12} \rightarrow 0$ as $1/L \rightarrow 0$, which in turn implies there is a paramagnetic phase for $T \gtrsim 0.9$.

It is interesting to compare the above results with the ones we obtained for 2D. Plots of u_{12} vs T are shown in Fig. 6 for various system sizes. Data points for \tilde{u}_{12} are also shown for $L = 16$. In contrast with the results for 3D, the three curves in Fig. 6 appear to come together only gradually, as $T \rightarrow 0$. Plots (not shown) of u_{12} vs $1/L$, can be made from the the data points shown in Fig. 6. One can then extrapolate u_{12} to $1/L \rightarrow 0$. At least for $0.2 \lesssim T$, $u_{12} \rightarrow 0$, which is consistent with a paramagnetic phase.

We can obtain ξ (of an infinite size system) making use of the data for u_{12} and of the fact that, according to FSS,^{34,35} u_{12} is only a function of ξ/L . Note that ξ/L is constant for any horizontal line that intersects the all the curves in either Fig. 5 or Fig. 6. We can thus obtain, $\xi(T_n)/L_n = c$, where c is some constant and T_n and L_n are the values of T and L where a horizontal line crosses the n th curve in Figs. 5 or 6. Different horizontal lines give different values of c which can be chosen independently in order to collapse all plots of ξ vs T into a single ξ vs T curve. Thus, we obtain the plots shown in Figs. 7 and 8.

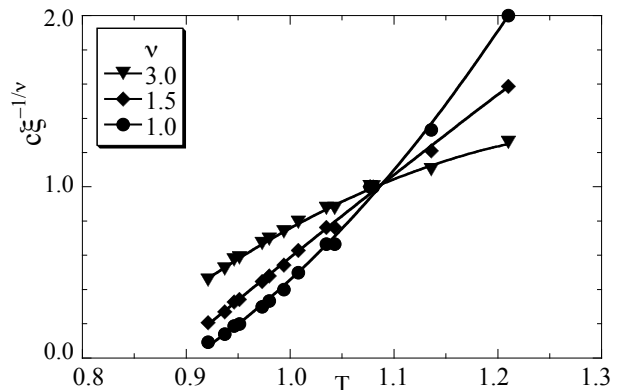


FIG. 7: Plots of $c\xi^{-1/\nu}$ vs T for 3D and the values of ν that are given in the graph. c is some undetermined constant. Lines are guides to the eye.

Extrapolations in plots such as the ones shown in Fig.7 give $T_c \simeq 0.88$ for 3D. From the errors in the data for u_{12} , we estimate an error $\delta T_c = 0.05$. We determine the exponent ν , in $\xi \sim (T - T_c)^{-\nu}$, from these plots. The value $\nu \simeq 1.5$ gives the best straight line fit in the $0.88 < T < 1.2$ range. On this basis we adopt the value $\nu \simeq 1.5$. Fits obtained from ν values outside the $1 \lesssim \nu \lesssim 2$ range show significant curvature, whence we assign the error $\delta\nu = 0.5$. Proceeding similarly for 2D, using plots as the ones shown in Fig. 8, we obtain $T_c \simeq 0$, though a spin glass phase below $T \simeq 0.1$ is conceivable, and $\nu = 3 \pm 1$.

From different extrapolation procedures we have arrived at values of T_c in the $[0.83, 0.88]$ range. Considering all the errors involved, we arrive at

$$T_c = 0.86 \pm 0.07 \quad (9)$$

for the RAD model in 3D.

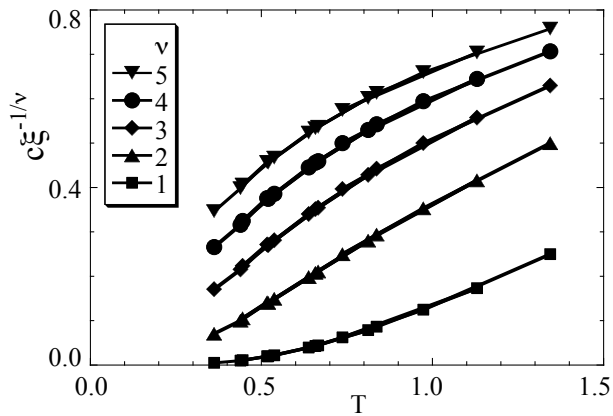


FIG. 8: Plots of $c\xi^{-1/\nu}$ vs T for 2D the values of ν that are given in the graph. c is some undetermined constant. Lines are guides to the eye.

IV. CONCLUSIONS

In sum, we have studied the equilibrium behavior of the RAD model by means of tempered Monte Carlo simulations. The sizes of the systems we have simulated, temperatures, as well as other parameters, are given in Table I. From them, we have drawn quantitative evidence that points to the following conclusions. In 3D, the paramagnetic phase covers the $T > T_c$ range, where $T_c = 0.86 \pm 0.07$. For $T < T_c$, there is a spin glass phase. In it, the overlap parameter, defined in Sec. II C, does not vanish. It is approximately given by Eq. (6). No in-

formation about critical behavior should be drawn from this equation, because it is not sufficiently accurate for it. From extrapolations of q_2 and q_1^2 to the $1/L \rightarrow 0$ limit (see Fig. 3), one might be tempted to infer that q_2 and q_1^2 become then equal, as in the droplet model. However, plots of u_{12} vs T , shown in Fig. 5, do not provide firm support for such a conclusion, because the $L \rightarrow \infty$ limit of u_{12} in the spin glass phase seems uncertain. We can only be reasonably sure that the limit is somewhere between the value of u_{12} shown for $L = 12$ and 1. From this, Eq. (8), which does not discriminate between the applicability of the droplet²⁴ or RSB²⁶ pictures to the RAD model, follows. Results for the correlation length ξ , exhibited in Fig. 7, are consistent with $\xi \sim (T - T_c)^{-\nu}$, where $\nu = 1.5 \pm 0.5$.²⁷

In 2D, the paramagnetic phase covers the $T \gtrsim 0$ range, though we cannot rule out a spin glass phase below $T \simeq 0.1$. Results for ξ , exhibited in Fig. 8, are consistent with $\xi \sim T^{-\nu}$, where $\nu = 3 \pm 1$.

Acknowledgments

We had interesting discussions with J. J. Alonso. We are indebted to the BIFI Institute (at Universidad de Zaragoza) and to the Carlos I Institute (at Universidad de Granada) for letting us run on many of their cluster nodes for months, and for financial support from Grant No. FIS2006-00708, from the Ministerio de Educación y Ciencia of Spain.

* E-mail address: jefe@Unizar.Es

¹ J. A. Mydosh, in *Magnetism and Magnetic Materials-1974*, edited by C. D. Graham, Jr., G. H. Lander, and J. J. Rhyne, AIP Conference Proceedings No. 24 (American Institute of Physics, New York, 1975), p. 131.
² N. Kawashima and A. P. Young, *Phys. Rev. B* **53**, R484 (1996); M. Palassini and S. Caracciolo **82**, 5128 (1999).
³ H. G. Ballesteros, A. Cruz, L. A. Fernández, V. Martín-Mayor, J. Pech, J. J. Ruiz-Lorenzo, A. Tarancón, P. Téllez, C. L. Ullod, and C. Ungil, *Phys. Rev. B* **62**, 14237 (2000); for a critical study, see H. Bokil, B. Drossel, and M. A. Moore, *Phys. Rev. B* **62**, 946 (2000).
⁴ L. W. Lee and A. P. Young, *Phys. Rev. Lett.* **90**, 227203 (2003); K. Hukushima and H. Kawamura, *Phys. Rev. B* **72**, 144416 (2005); I. A. Campbell and H. Kawamura, *Phys. Rev. Lett.* **99**, 019701 (2007); I. Campos, M. Cotallo-Aban, V. Martín-Mayor, S. Pérez-Gaviro, and A. Tarancón, *Phys. Rev. Lett.* **97**, 217204 (2006); *ibid* **99**, 019702 (2007).
⁵ L. W. Lee and A. P. Young, *Phys. Rev. B* **76**, 024405 (2007).
⁶ J. L. Dormann, L. Bessais, and D. Fiorani, *J. Phys. C* **21**, 2015 (1988); T. Shinjo, *Surf. Sci. Rev.* **12**, 51 (1991); F. Bødker, S. Mørup, and S. Linderorth, *Phys. Rev. Lett.* **72**, 282 (1994); S. Mørup, F. Bødker, P. V. Hendriksen, and

S. Linderorth, *Phys. Rev. B* **52**, 287 (1995); X. Batlle and Amílcar Labarta, *J. Phys. D: Appl. Phys.* **35**, R15 (2002).
⁷ For an ordered assembly, see, R. F. Wang, C. Nisoli, R. S. Freitas, J. Li, W. McConville, B. J. Cooley, M. S. Lund, N. Samarth, C. Leighton, V. H. Crespi, and P. Schiffer, *Nature* **439**, 303 (2006).
⁸ J. Snider and C. C. Yu, *Phys. Rev. B* **72**, 214203 (2005).
⁹ See, for instance, J. F. Fernández and J. J. Alonso, *Phys. Rev. B* **62**, 53 (2000).
¹⁰ W. Luo, S. R. Nagel, T. F. Rosenbaum, and R. E. Rosensweig, *Phys. Rev. Lett.* **67**, 2721 (1991); F. Bert, V. Dupuis, E. Vincent, J. Hammann, and J.-P. Bouchaud, *Phys. Rev. Lett.* **92**, 167203 (2004); V. S. Zotev, G. F. Rodriguez, G. G. Kenning, R. Orbach, E. Vincent and J. Hammann, *Phys. Rev. B* **67**, 184422 (2003); G. G. Kenning, G. F. Rodriguez, and R. Orbach, *Phys. Rev. Lett.* **97**, 057201 (2006).
¹¹ T. Jonsson, J. Mattsson, C. Djurberg, F. A. Khan, P. Nordblad, and P. Svedlindh, *Phys. Rev. Lett.* **75**, 4138 (1995).
¹² T. Jonsson, P. Nordblad, and P. Svedlindh, *Phys. Rev. B* **57**, 497 (1998).
¹³ J.-O. Andersson, C. Djurberg, T. Jonsson, P. Svedlindh, and P. Nordblad, *Phys. Rev. B* **56**, 13 983 (1997).
¹⁴ M. Ulrich, J. García-Otero, J. Rivas, and A. Bunde, *Phys.*

- Rev. B **67**, 024416 (2003).
- ¹⁵ O. Iglesias and A. Labarta, Phys. Rev. B **70**, 14 4401 (2004).
- ¹⁶ S. Russ and A. Bunde, Phys. Rev. B **75**, 174445 (2007).
- ¹⁷ Aging is the effect that waiting (after cooling to some fixed temperature) a time t_w before a field is applied has on the subsequent evolution of the magnetization. It was first observed in spin glasses by, L. Lundgren, P. Svedlindh, P. Nordblad, and O. Beckman, Phys. Rev. Lett. **51**, 911 (1983); see also, R. V. Chamberlin, Phys. Rev. B **30**, 5393 (1984); for a more recent account, see, for instance, G. G. Kenning, G. F. Rodriguez, and R. Orbach, Phys. Rev. Lett. **97**, 057201 (2006).
- ¹⁸ R. B. Harris, M. Plischke, and M. J. Zuckerman, Phys. Rev. Lett. **31**, 160 (1973); see also, B. Dieny and B. Barbara, Phys. Rev. Lett. **57**, 1169 (1986).
- ¹⁹ Bulk anisotropy energies ε_a are most often larger than nn dipole-dipole energies ε_d (see, R. M. Bozorth *American Institute of Physics Handbook* (McGraw-Hill, Inc., New York, 1957), tables 5h-16 and 5h-17, pp 5-221, 5-222. In ferrofluids, nanoparticle concentration enables control of $\varepsilon_a/\varepsilon_d$ ¹¹. In closely packed nanoparticle arrays, $\varepsilon_a/\varepsilon_d$ is volume independent, but surface effects can raise anisotropy energies hugely.
- ²⁰ C. Jayaprakash and S. Kirkpatrick, Phys. Rev. B **21**, 4 072 (1980).
- ²¹ M. A. Zaluska-Kotur and M. Cieplak, Europhys. Lett. **23**, 85 (1993).
- ²² K. Hukushima and K. Nemoto, J. Phys. Soc. Jpn. **65**, 1604 (1996); E. Marinari, *Advances in Computer Simulation*, edited by J. Kertész and Imre Kondor (Springer-Verlag, Berlin, 1998), p. 50; cond-mat/9612010.
- ²³ N. A. Metropolis, A. W. Rosenbluth, M. N. Rosenbluth, A. H. Teller, and E. Teller, J. Chem. Phys. **21**, 1087 (1953).
- ²⁴ D. S. Fisher and D. A. Huse, J. Phys. A **20**, L1005 (1987); D. A. Huse and D. S. Fisher, *ibid.* **20**, L997 (1987); D. S. Fisher and D. A. Huse, Phys. Rev. B **38**, 386 (1988).
- ²⁵ H. G. Katzgraber, M. Palassini, and A. P. Young, Phys. Rev. B, **63**, 184422 (2001).
- ²⁶ G. Parisi, Phys. Rev. Lett. **43**, 1754 (1979); *ibid* **50**, 1946 (1983); For reviews, see M. Mzard, G. Parisi, and M. A. Virasoro, *Spin Glass Theory and Beyond* (World Scientific, Singapore, 1987); E. Marinari, G. Parisi, and J. J. Ruiz-Lorenzo, in *Spin Glasses*, edited by K. H. Fischer and J. A. Hertz, (Cambridge University Press, Cambridge, 1991).
- ²⁷ This value of ν is within the range of the long list of values that have been obtained for short range Ising models with various random bond distributions.³⁵ Screening of the (long ranged) dipolar interactions might bring this about.
- ²⁸ J. J. Alonso and J. F. Fernández, Phys. Rev. B **74**, 184416 (2006).
- ²⁹ J. F. Fernández and J. J. Alonso, Phys. Rev. B **76**, 014403 (2007).
- ³⁰ R. B. Griffiths, Phys. Rev. **176**, 655 (1968).
- ³¹ S. F. Edwards and P. W. Anderson, J. of Phys F **5**, 965 (1975).
- ³² q_1 has been used before, see for instance, A. T. Ogielski, Phys. Rev. B **32**, 7384 (1985).
- ³³ J. M. Kosterlitz and D. J. Thouless, J. Phys.C **6**, 1181 (1973); J. M. Kosterlitz, *ibid.* **7**, 1046 (1974).
- ³⁴ M. P. Nightingale, J. Appl. Phys. **53** 7927 (1982); M. N. Barber, in *Phase Transitions and Critical Phenomena*, edited by C. Domb and J. Lebowitz (Academic, New York, 1983), Vol. 8.
- ³⁵ H. G. Katzgraber, M. Körner, and A. P. Young, Phys. Rev. B **73**, 224432 (2006).
- ³⁶ M. S. S. Challa, D. P. Landau, and K. Binder, Phys. Rev. B **34**, 1841 (1986).